# Airflow and Particle Deposition in a Dry Powder Inhaler
## *A CFD Simulation*

J. Milenkovic[1], A. H. Alexopoulos[1] and C. Kiparissides[2]
[1]*CPERI, CERTH, 6th km Harilaou-Thermi rd., Thermi, Greece*
[2]*Department of Chemical Engineering, Aristotle University of Thessaloniki, Thessaloniki, Greece*

Keywords: Dry Powder Inhaler, Turbuhaler, CFD, Particle, Deposition.

Abstract: In this work the steady-state flow in a commercial dry powder inhaler device (i.e., Turbuhaler) is described. The DPI geometry is constructed in a CAD/CAM environment (i.e., CATIA v5) and then imported into GAMBIT where the geometry is discretized into a computational grid. The Navier-Stokes equations are solved using FLUENT (v6.3) considering different flow models, i.e., laminar, k-ε, k-ε RNG, and k-ω SST. Particle motion and deposition are described using an Eulerian-fluid/Lagrangian-particle approach. Flow and particle deposition for a range of mouthpiece pressure drops (i.e., 800-8800Pa), as well as particle sizes corresponding to single particles and aggregates (i.e., 0.5-20μm) are examined. The total volumetric outflow rate, the overall particle deposition as well as the particle deposition sites in the DPI are determined. The transitional k-ω SST model for turbulent flow was found to produce results most similar to a reference Large Eddy Simulation solution as well as experimental results for the pressure drop in the DPI. Realistic particle deposition results could only be obtained by considering a nonideal sticking coefficient corresponding to a critical capture velocity of 2.7m/s. Overall, the simulation results are found to agree well with available experimental data for volumetric flow and particle deposition.

## 1 INTRODUCTION

Dry Powder Inhalers "DPI"s are one of the principle means of delivering pharmaceuticals due to their ease of use and cost-effectiveness. The main function of a DPI device is the adequate dispersion and delivery of particles. Initially the particles are in the form of a loose powder which, under the action of airflow is broken up and dispersed as particle aggregates which are then further broken up into fine particles (Ashurst et al. 2000); (Newman and Busse, 2002); (Tobyn et al., 2004); (Islam et al., 2008); (Alagusundaram et al., 2010). Powder properties, e.g., cohesion, charge, size, and size distribution, influence powder dispersion and the breakage of particle agglomerates (French et al., 1996); (Zeng et al., 2000); (Finlay, 2001); (Newman and Busse, 2002); (Chan, 2006).

One of the common problems with DPIs is the loss of powder/drug due to deposition within the device. In order to provide the maximum drug dose per inhalation and to ensure minimal dose-to-dose variation it is necessary to minimize the drug losses due to internal deposition. It is also desired to have good control over the dispersibility of the powder, release of drug (when attached to powder particles), and breakup of agglomerates in order to achieve the desired particle/agglomerate size distributions at the DPI mouthpiece outflow (Alagusundaram et al., 2010). Consequently, if the underlying processes are better understood one can achieve the desired outflow particle distribution which will conceivably minimize oropharyngeal losses and also permit better targeting for drug delivery in the respiratory tract.

Due to the complex and transient flow structures observed in most commercial DPIs as well as the dynamic powder breakup and dispersion processes only a small number of Computational Fluid Dynamics "CFD" investigations have been conducted (Schuler et al., 1999); (Ligotke, 2002). Systematic computational studies have led to a better understanding of the function of DPI devices. For example, Coates et al. (2004, 2005, 2006) studied the Aerolizer DPI in detail including the effects of air-intake, mouthpiece, and internal grid which led to improvements in the design and function of the DPI. Recently, the discrete element method, DEM,



Milenkovic J., H. Alexopoulos A. and Kiparissides C..
Airflow and Particle Deposition in a Dry Powder Inhaler - A CFD Simulation.
DOI: 10.5220/0004058102500259
In *Proceedings of the 2nd International Conference on Simulation and Modeling Methodologies, Technologies and Applications* (SIMULTECH-2012), pages 250-259
ISBN: 978-989-8565-20-4

coupled to continuous phase-models has been implemented to describe the powder dispersion process within the inhaler (Tong et al., 2010); (Calvert et al., 2011). From the current state-of-the-art it is clear that the proper description of the agglomerate strength as well as the particle/agglomerate interaction with the inhaler walls are key processes that determine the final dispersion and size distribution of pharmaceutical powders (Adi et al., 2011).

The Turbuhaler (AstraZeneca) is a multidose dry powder inhaler that is widely used to deliver a number of drugs (typically for asthma), e.g., terbutaline sulphate, (as Bricanyl), or budesonide (as Pulmicort), to the upper respiratory tract (Wetterlin, 1988). Each dose is initially in the form of loosely packed particle agglomerates, ~10-20μm in size, which are released into a mixing/dispersion chamber, where they are broken up into particles, ~1μm in size, which are then directed to the inhalation channel of the device (Tsima et al., 1994; Wetterlin, 1988). The proper function of the Turbuhaler is dependent on the dynamic volumetric flow as well as the peak inspiratory flow rate attained during inhalation, the amount of particles lost due to deposition within the device, and the adequate dispersion and breakup of the powder agglomerates in the airflow exiting the mouthpiece. Recent experimental investigations have provided detailed information on particle capture as well as the percent and size distribution of escaped particles in the outlet flow (de Koning et al., 2001); (Hoe et al., 2009); (Abdelrahim, 2010).

In this work the steady airflow in a Turbuhaler DPI is determined by CFD simulations and particle motion as well as deposition is determined by Eulerian-fluid/Lagrangian-particle simulations. In what follows the DPI geometry, the discretization procedure, and the CFD simulations are described in detail. Next the results for steady-state airflow are presented follow by the results for particle deposition. Finally, the computational results are compared to available experimental data.

## 2 RESULTS

The Turbuhaler DPI geometry was constructed in a CAD/CAM environment (i.e., CATIA v5 R19) and then imported into GAMBIT (v2.1) where a series of computational grids were constructed consisting of 2 $10^5$ – 2 $10^6$ tetrahedral cells with a maximum skewness of 0.85 (Figures 1, 2, and 3). The computational grids were originally refined in regions where large gradients of flow were expected.

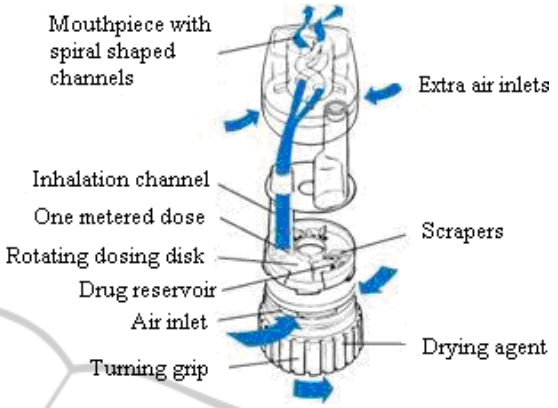


Figure 1: Turbuhaler dry powder inhaler.

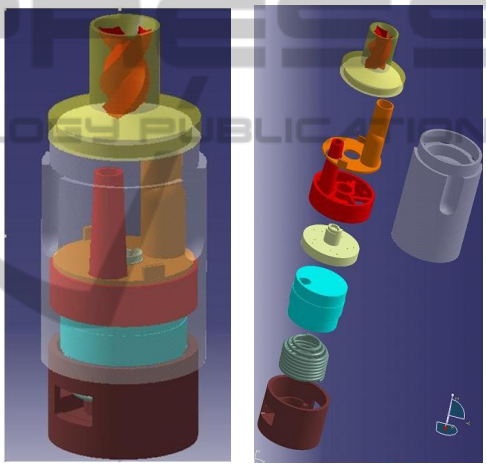

Figure 2: Turbuhaler dry powder inhaler CAD geometry.

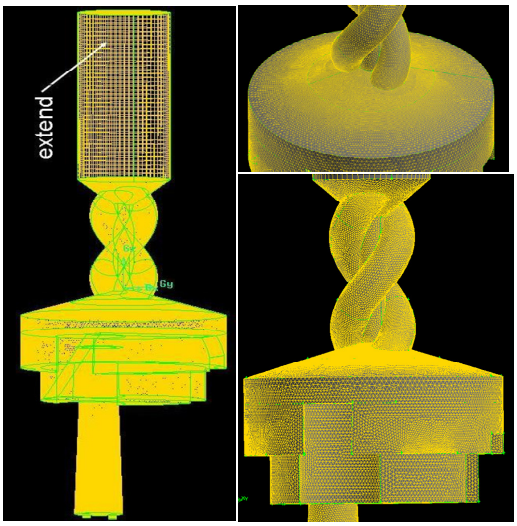


Figure 3: Turbuhaler Dry Powder Inhaler Computational Grid (1 $10^6$ tetrahedral cells).

Further refinement was conducted within FLUENT based on actual velocity gradients observed in initial solutions.

The Navier-Stokes equations for airflow were solved using the commercial CFD software (i.e., FLUENT v6.3). The SIMPLEC scheme was employed to describe pressure-velocity coupling. Second order discretization was used for pressure and third order MUSCL for momentum and turbulent variables. Convergence of CFD simulations was assumed when the residuals were < $10^{-4}$. Zero gauge pressure boundary conditions were employed at all the inflows, i.e., two powder loaded cylinders (see bottom of Figure 3a) and four extra air inlets in the DPI dispersion chamber (see Figure 1). Different steady state airflows were simulated by imposing a wide range of pressure drops at the mouthpiece outflow ranging from 800 to 8800Pa corresponding to volumetric flow rates of 20 to 70 l/min. Steady-state airflow can be considered an approximation to dynamic inhalations where the flow rate has approached the peak inspiratory value.

Eulerian-fluid/Lagrangian-particle simulations of particle motion and deposition were conducted for particles between 0.5-20μm in size encompassing the single particle and particle agglomerate size ranges of typical pharmaceutical powders employed in the Turbuhaler. Particles were assumed to be released instantaneously at t = 0 and uniformly from a surface located immediately upstream from the powder storage site. Powder dispersion was assumed to occur instantaneously after which no further breakage occurred. Consequently, particles in motion were taken to be constant in size. Upon collision with the inhaler walls particles either deposited or reflected. No collision-induced breakage was examined in this work. The capture efficiency of particles with the inhaler walls was assumed to be either equal to one or a function of the velocity magnitude.

## 2.1 Simulations of Airflow in the Turbuhaler DPI

According to the range of volumetric airflows examined in this work, e.g. Q = 20 - 70l/min, the local Reynolds numbers, $Re = Q \rho / \mu A^{1/2}$, where ρ and μ are the density and the viscosity of air and A is the cross-sectional area, ranged from 130-16,000. Consequently the transitional SST k-ω model was employed to describe the transitional turbulent flows encountered in the DPI.

Computational grids, varying between 2 $10^5$ and 2 $10^6$ tetrahedral elements, were employed to test for convergence. The 1 $10^6$ grid was found to provide essentially identical results as the 2 $10^6$ grid and was used for the results presented in this paper. It should be noted that the computational grid was extended from the mouthpiece by 20mm in order to minimize recirculation effects at the outflow surface and to improve convergence behaviour.

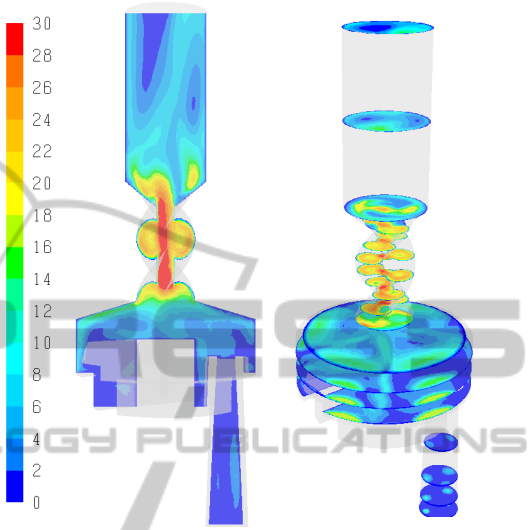


Figure 4: Velocity magnitude in the Turbuhaler DPI (mouthpiece pressure drop ΔP = 800Pa).

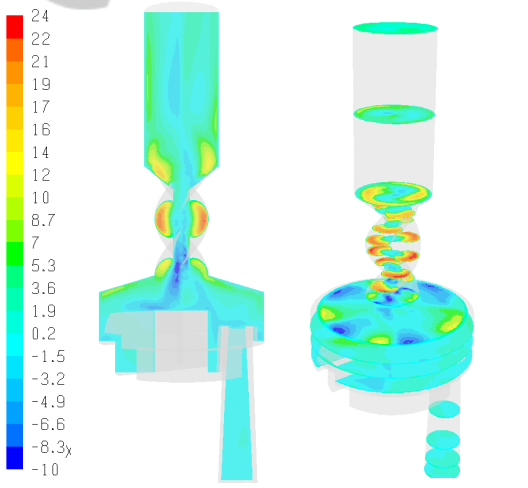


Figure 5: Tangential velocity in the Turbuhaler DPI (ΔP = 800Pa).

In Figures 4-6 the velocity magnitudes as well as the tangential and radial velocities are displayed along an axial (i.e., zx) plane and several planes normal to the z-axis (i.e., xy sections). As can be observed, the airflow in the DPI device is found to be laminar in the inhalation channel with two jet flows emanating from the powder storage cylinders.

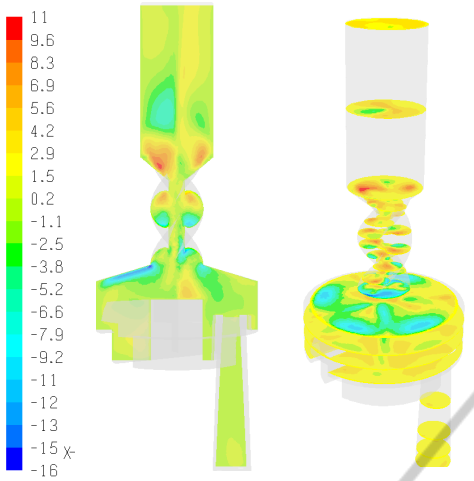


Figure 6: Radial velocity in the Turbuhaler DPI (ΔP = 800Pa).

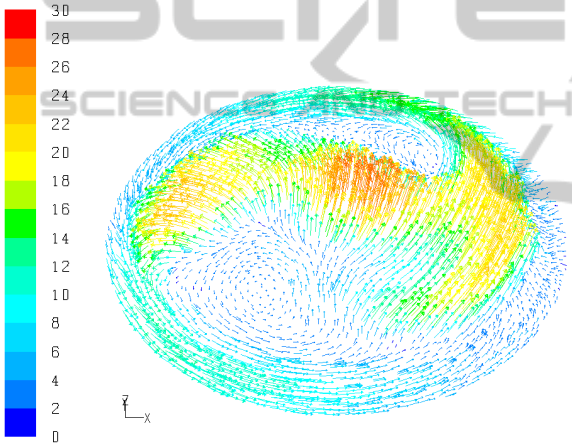


Figure 7: Mouthpiece velocity vectors (ΔP = 800Pa).

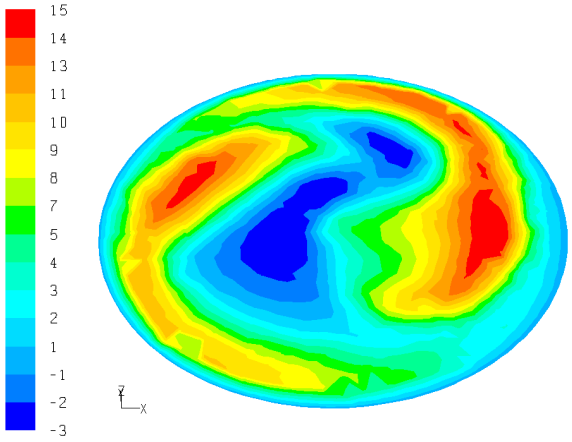


Figure 8: Mouthpiece tangential velocity contours (ΔP = 800Pa).

In the dispersion chamber the flow is characterized by large eddies and secondary flows. In the helical region significant tangential flows develop and persist about halfway up the mouthpiece extension. The tangential motion induced by the helical airway in the mouthpiece is significant reaching 83% of the maximum velocity magnitude. It should be noted that the velocity profiles observed for larger flow rates, e.g., 60 l/min, are qualitatively similar.

The mouthpiece outflow of a DPI is very important as it determines the dispersion and flow behaviour of the particles in the oral cavity and the upper respiratory tract and consequently influences particle losses in the oral cavity and throat regions. In Figures 7 and 8 the mouthpiece outflow for a pressure drop of ΔP = 800Pa is shown in terms of velocity magnitude and tangential velocity. It is clear that the flow is strongly influenced from the preceding helical region and that the axial and tangential components of the velocity are nonuniform. Moreover, the strongly localized tangential and axial airflows at the mouthpiece cause recirculation flows in both the tangential and axial directions, further complicating the flow.

Large Eddy Simulations “LES” fully resolve the large scale motion of turbulent flows thus providing more information and accurate results compared to Reynolds Averaged Navier-Stokes “RANS” approaches, e.g., k-ε, k-ω. The computational burden of LES is significant (e.g., at least an order of magnitude more than with RANS models). Consequently, only a single case (i.e., ΔP = 800Pa) of steady-state flow in the Turbuhaler DPI was simulated with LES using FLUENT.

In Figure 9 the results for the mean velocity magnitude obtained with LES is shown. The main flow structures are similar with the k-ω SST results in Figure 4 but, as expected, differences can be observed in the flow details as well as in secondary flows.The enhanced resolution of eddies and secondary flows with the LES is demonstrated in Figures 10 and 11 depicting the tangential and radial flow, respectively. Compared to the radial and tangential flows predicted with the k-ω SST model (Figures 6 and 7) there are many differences, e.g., in the large eddies of the mouthpiece extension.

In Figure 12 the magnitude of the RMS velocity fluctuations in the DPI is shown. Significant velocity fluctuations are observed at the top of the dispersion chamber (~6m/s) and in the mouthpiece extension (~9m/s). The intensity of fluctuations (e.g., RMS velocity / velocity magnitude) varies within the device up to a value of ~50% indicating significant local fluctuations around the mean for the length fluctuations of the individual velocity components

scales of flow resolved within the LES. The RMS range from 1-8m/s for the axial velocity component and 1-4m/s for the other components with different spatial variations within the device. These results demonstrate that the fundamental assumption of local turbulence isotropy of the RANS models is incorrect In Figure 13 the tangential velocities at the outlet surface for ΔP = 1400Pa are shown. It is clear that the tangential velocities predicted by the k-ω SST and LES turbulence models are very similar. In fact the k-ω SST turbulence model provided the most similar to the LES results compared to the other RANS turbulence models (e.g., standard k-ε, RNG k-ε). Consequently, despite the observed differences in secondary flows (Figures 9-11) the k-ω SST model was employed for all the simulations of this work

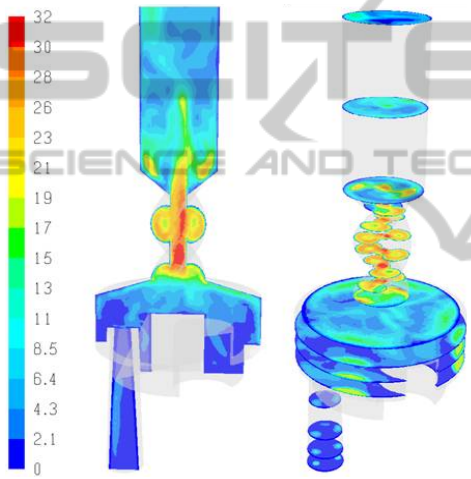


Figure 9: Velocity magnitude in the Turbuhaler DPI – LES results (ΔP = 800Pa).

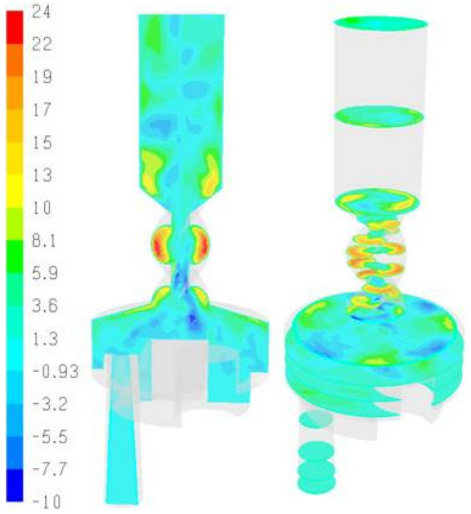


Figure 10: Tangential velocity component in the Turbuhaler DPI – LES results (ΔP = 800Pa).

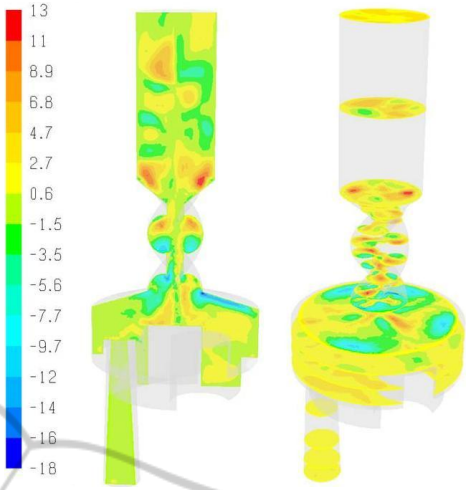


Figure 11: Radial velocity component in the Turbuhaler DPI – LES results (ΔP = 800Pa).

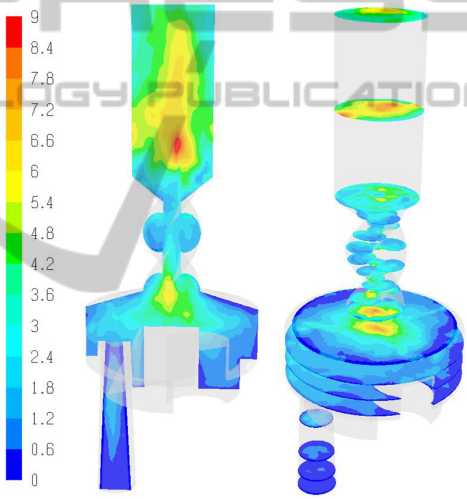


Figure 12: RMS velocity magnitude in the Turbuhaler DPI (ΔP = 800Pa).

## 2.2 Simulation of Particle Motion and Deposition in the Turbuhaler DPI

Eulerian-fluid/Lagrangian-particle simulations were performed for all the flows examined in section 2.1. These simulations are generally valid for particle volume fractions <10%. For effective powder dispersion the solids volume ratio in the DPI device is approximately $10^{-2}$-$10^{-4}$ depending on the location and the flow rate. Consequently, the particle phase was assumed to not influence the airflow.

The total particle deposition in the DPI device was determined assuming either a 100% capture efficiency, σ, or a capture efficiency based on a critical velocity magnitude. The later case was

implemented within FLUENT using a user-defined function for the capture efficiency based on the normal velocity of the particle at the moment of collision with the walls.

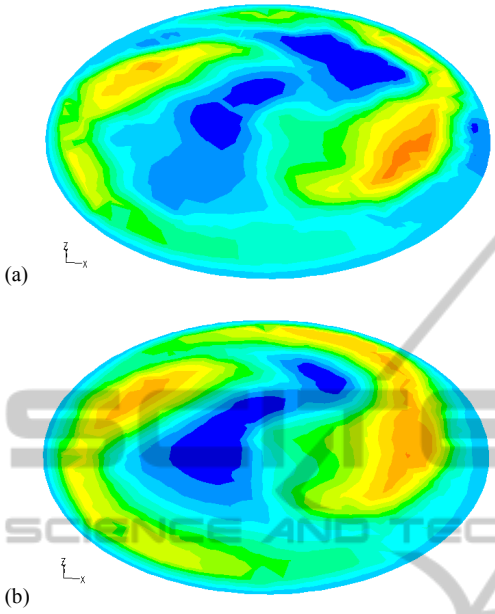


Figure 13: Tangential velocity component at the mouthpiece exit (ΔP = 1400Pa). (a) LES (b) k-ω SST.

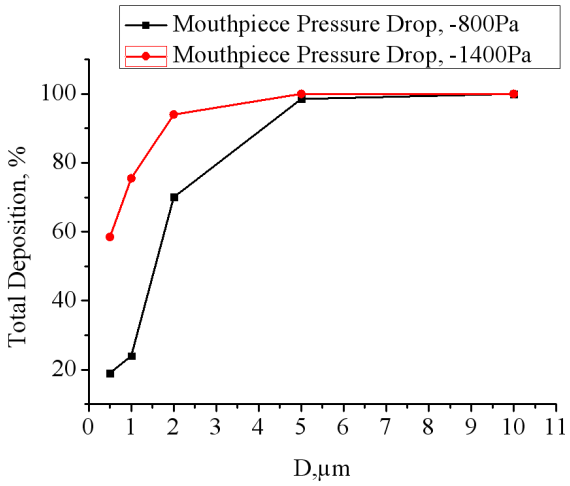


Figure 14: Overall particle deposition in the Turbuhaler.

Single-sized simulations were performed with particles ranging from 0.5-20µm. Particle sizes 0.5-1.5µm correspond to individual particle constituents of the agglomerates. Agglomerate breakage and redispersion effects were not considered. Instead, the agglomerates in the powder storage cylinders were assumed to break-up rapidly into their constituent particles. Clearly, agglomerate breakage and flow occur simultaneously and this is an area which requires further investigation.

For micron sized particles inertial forces dominate the deposition process and for particles <100µm gravity can be ignored during the time-scale of a single inhalation. In Figure 14 the total deposition for single-sized particles ranging from 0.5-10µm, for an ideal capture efficiency, i.e., σ = 1, and for two pressure drops, e.g., 800 and 1400Pa, are shown. These simulation results indicate that for a pressure drop of 800Pa the deposition of 0.5-1µm particles is 19-24% but that of agglomerates 5-10µm is 90-100%. The predicted total particle deposition in the DPI increases with volumetric flow to large, and unrealistic, values (Figure 14). Smaller deposition values can be obtained by considering less than 100% particle capture efficiency. Other mechanisms such as agglomerate breakage dynamics and/or redispersion of deposited agglomerates could also result in smaller values of particle deposition.

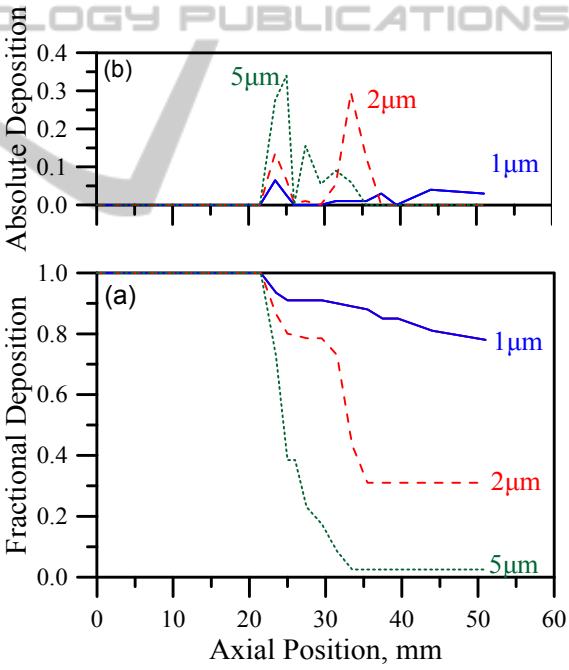


Figure 15: Particle deposition. (a) Fractional cumulative deposition, (b) Local deposition (ΔP = 800Pa).

In Figure 15 the axial fractional cumulative deposition distribution and the local fractional deposition for ΔP = 800Pa are shown. The results indicate significant differences in the deposition patterns with particle size with most deposition occurring in the dispersion chamber and the helical region.

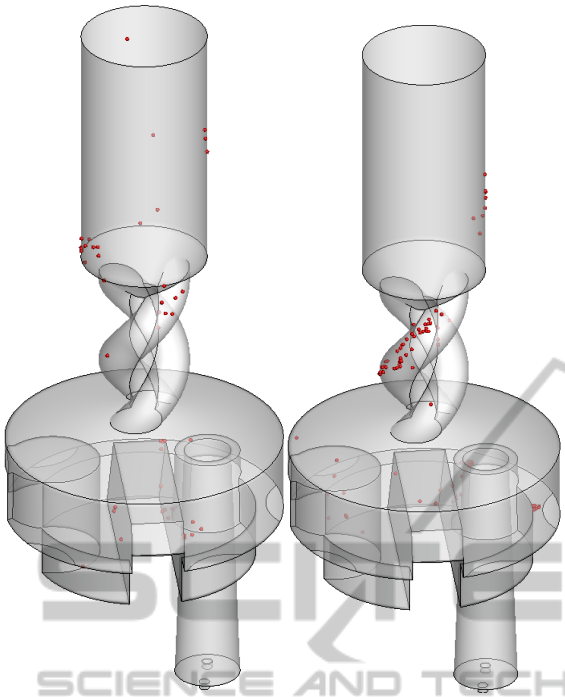

Figure 16: Particle Deposition – Effect of Pressure drop. (a) ΔP = 800Pa, (b) ΔP = 5400Pa. D = 1μm. σ = 1.

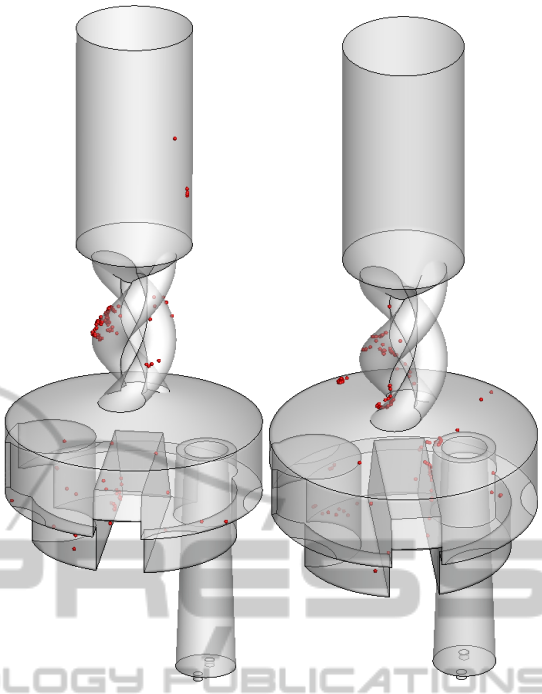

Figure 17: Particle Deposition – Effect of Particle Size. (a) D = 2 μm, (b) D = 5 μm. ΔP = 800Pa. σ = 1.

The spatial distribution of particles deposited on the DPI walls was visualized using Tecplot. In Figure 16 particle depositions for two pressure drops, i.e., 800 and 5400Pa, are shown. It is clear that the larger pressure drop results in increased velocities and total particle deposition but also significantly different particle deposition patterns. The increased deposition for large pressure drops in the helical region is caused by the increased tangential flow in this region.

In Figure 17 the effect of particle size on the distribution of deposited particles in the DPI device is shown. Comparing particle sizes of 1 (see Figure 16a), 2 and 5μm (Figure 17) significant differences in the total deposition as well as the deposition distribution are observed. The significant particle deposition that occurs in the mouthpiece region (which includes the helical region) is actually a common problem in many commercial DPI devices where about half the internal deposition occurs (de Koning et al., 2001).

The results of Figures 16 and 17 can be used to optimize the design of the DPI. For example, the helical region of the Turbuhaler could be redesigned so that smaller radial and tangential velocities develop leading to decreased particle collisions in this region.

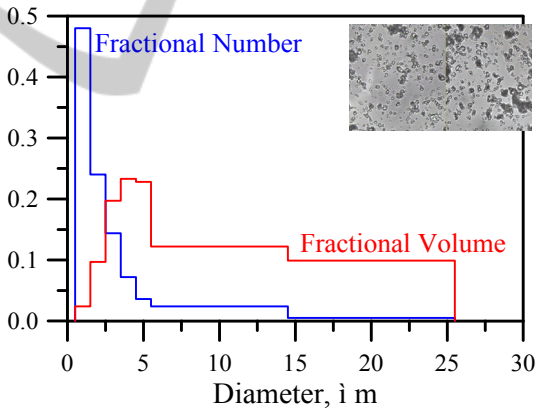


Figure 18: Fractional particle number and volume distrbution. Inset photo 120x80μm.

Figure 18 displays the particle size distribution of freely flowing powder containing Budesonide (Pulmicort). The peak in the number distribution is at $D_0$=2.2μm while for the volume distribution it is at 4.5μm. It was found that a Rosin Rammler distribution, f(D), with a shape parameter value of n = 1 and a mean diameter of $D_0$ = 2.2μm, i.e.,

$$f(D) = (1/D_0)e^{-D/D_0} \quad (1)$$

is a good approximation to the distribution depicted in Figure 18. The injected, escaped and deposited fractional volume distributions for ΔP = 800Pa are

provided in Figure 19. It is observed that, due to the size-dependent deposition efficiency, the particle distribution exiting the device is significantly different than the injected particle distribution. The shape of the injected particle size distribution affects the total number of particles deposited in the DPI device due to the different number of large particles which deposit to a larger degree (Table 1).

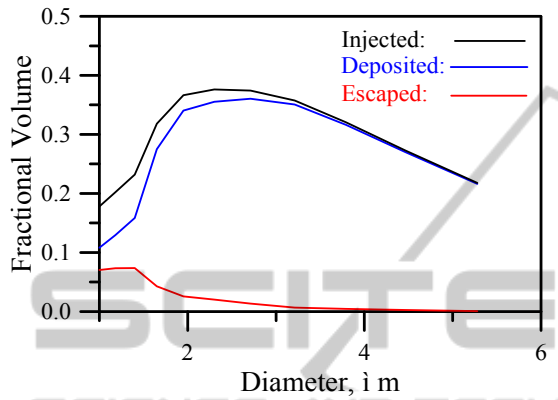


Figure 19: Particle Deposition. (a) Fractional Cumulative Deposition, (b) Local.Deposition (ΔP = 800Pa).

Table 1: Particle deposition. Effect of injected particle distribution. (RR Log = Rosin Rammler logarithmic)

| # | Number Injected | Number Deposited | % Deposited |
|---|---|---|---|
| Single-size | 248 | 195 | 78.6 |
| RR Log | 2480 | 2059 | 83.0 |
| RR Log | 4712 | 3970 | 84.2 |
| RR Linear | 18848 | 17981 | 95.4 |

## 2.3 Comparison to Experimental Data

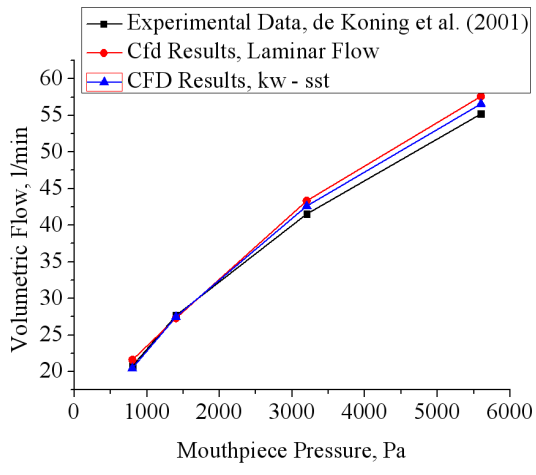


Figure 20: Volumetric flow in the Turbuhaler.

The computational results of this work were compared to the experimental results of de Koning et al (2001) and Abdelrahim (2010) for the Turbuhaler in terms of flow and particle deposition.

In Figure 20 the predicted steady-state volumetric flows are plotted against the outlet pressure drop applied at the mouthpiece. Both laminar and k-ω SST models for flow are examined. It is clear that both models agree very well with the experimental data for all flow rates with the k-ω SST model being slightly more accurate.In this work the capture efficiency is related to a critical normal velocity, $v_c$, above which particles reflect (assuming no dissipation of momentum). The developed by Brach and Dunn (1992). According to this model the critical normal velocity is.

$$v_c = \left(\frac{2E}{D}\right)^{10/7} \quad (2)$$

where D is the particle diameter and the effective stiffness parameter E is given by

$$E = 0.51\left(\frac{5\pi^2(k_s + k_p)}{4\rho^{3/2}}\right)^{2/5} \quad (3)$$

and ks kp are determined by:

$$k_s = \frac{1-\nu_s^2}{\pi E_s} \text{ and } k_p = \frac{1-\nu_p^2}{\pi E_p} \quad (4)$$

where $\nu_s$ and $\nu_p$ and $E_s$ and $E_p$ are the Poisson's ratio and Young's modulus of the surface and particle, respectively.

In the case of lactose particles ($\nu_p$=0.4 and $E_p$=1.0GPa) colliding with polystyrene surfaces ($\nu_s$=0.35 and $E_s$ =4.1GPa) the critical velocity was determined to be $v_c$ = 2.7m/s.

In Figure 21 the total, dispersion chamber, and mouthpiece particle depositions for 1400Pa (or 30 l/min) are compared to the experimental data of de Koning et al. (2001). This critical velocity value results in an overall capture efficiency of ~42.5%, the mouthpiece, dispersion chamber, and total particle deposition results for Q = 30 l/min are in good agreement to the experimental data. It should be noted that a 100% capture efficiency leads to very large total deposition values, i.e., 75%, for this flow rate (see Figure 14) and even larger for larger flow rates, e.g., Q>30 l/min.

In Figure 22 the predicted total particle deposition are compared to the experimental data of de Koning et al (2001) and Abdelrahim (2010) for flowrates Q = 30, 40, 50, 60 and 70 l/min and for two different inspired volumes, i.e., 2 and 4l

(Abdelrahim, 2010). For a critical velocity of $v_c$ = 2.7m/s and a particle diameter of D = 2μm the agreement with the experimental data is good considering the different experimental conditions (e.g., dynamic inhalation vs. steady state simulations) and the simplicity of the particle deposition model (e.g., velocity cut-off capture efficiency and single-size size distribution). Different values of $v_c$ are also shown to provide an indication of the sensitivity of particle deposition on the value of $v_c$.

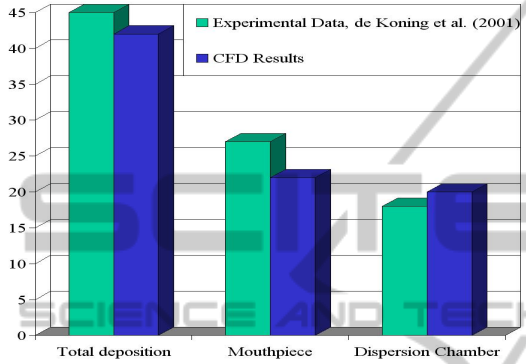


Figure 21: Regional particle deposition in the Turbuhaler. Q = 30 l/min. $v_c$ = 2.7m/s.

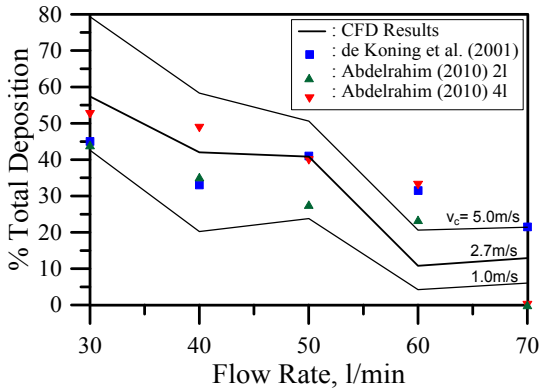


Figure 22: Total particle deposition in the Turbuhaler. D = 2 μm. $V_c$ = 2.7 m/s. Comparison between experimental results of de Koning et al. (2001), Abdelrahim (2010) and computational CFD results.

## 3 CONCLUSIONS

This work has demonstrated the use of CFD to determine the complicated airflow as well as particle motion and deposition in the Turbuhaler DPI. As the flow was either locally laminar or transitionally turbulent the transitional SST k-ω model for turbulence was employed. LES results revealed some differences in the large eddies and secondary flows but were otherwise closest to the k-ω SST results. The simulations revealed complicated flows with intense recirculation patterns in the dispersion chamber and strong tangential flows in the helical region of the mouthpiece.

Particle deposition was found to depend on size and flow rate and occurred predominantly in the dispersion chamber and the mouthpiece. The computational solutions were compared to experimental data for volumetric flow and regional deposition of de Koning et al. (2001) and good agreement was observed for volumetric flow. Particle deposition data were in agreement to experimental data only for capture efficiencies less than 100%. A simple collision model by Brach and Dunn (1992) was employed to determine the critical velocity for particle capture, i.e., $v_c$=2.7m/s, which was found to produce total particle depositions similar to the experimental values of de Koning et al (2001) and Abdelrahim (2010).

Future work will involve the simulation of dynamic inhalations and will elaborate on the particle collision model. The particle collision model can be extended by including the effects of particle properties (e.g., size, shape, and charge), surface properties (e.g., roughness, charge), as well as humidity.

## REFERENCES

Abdelrahim, M. E., (2010) Emitted dose and lung deposition of inhaled terbutaline from Turbuhaler at different conditions, *Respiratory Medicine*, 104, 682-689.

Alagusundaram M., N. Deepthi, S. Ramkanth, S. Angalaparameswari, T. S. M. Saleem, K. Gnanaprakash, V. S. Thiruvengadarajan, C. Madhusudhana, C. M. Alagusundaram et al., (2010) Dry Powder Inhalers - An Overview, *Int. J. Res. Pharm. Sci.*, 1(1), 34-42.

Ashurst I., A. Malton, D. Prime and B. Sumby, (2000) Latest advances in the development of dry powder inhalers, *PSTT*, 3(7), 246-256.

Brach RM, Dunn P.F (1992). A Mathematical Model of Impact and Adhesion of Microspheres. *Aerosol Sci. Technol.*, 23, 51-71.

Calvert G., A. Hassanpour, M. Ghadiri, (2011) Mechanistic analysis and computer simulation of the aerodynamic dispersion of loose aggregates, *Chemical Engineering Research and Design*, 89, 519–525.

Chan H-K, (2006) Dry powder aerosol drug delivery – Opportunities for colloid and surface scientists, *Colloids and Surfaces A: Physicochem. Eng. Aspects*, 284-285, 50-55.

Coates M. S., D. F. Fletcher, H-K. Chan and J. A. Raper, (2004) Effect of Design on the Performance of a Dry Powder Inhaler Using Computational Fluid Dynamics. Part 1: Grid Structure and Mouthpiece Length, *J. of Pharmaceutical Sciences*, 93, 2863–2876.

Coates M. S., H-K Chan, D. F. Fletcher and J. A. Raper, (2005) Influence of Air Flow on the Performance of a Dry Powder Inhaler Using Computational and Experimental Analyses, *Pharmaceutical Research*, 22(9), 923-932.

Coates M. S., H-K. Chan, D. F. Fletcher and J. A. Raper, (2006) Effect of Design on the Performance of a Dry Powder Inhaler Using Computational Fluid Dynamics. Part 2: Air Inlet Size, *J. of Pharmaceutical Sciences*, 95(6), 1382-1392.

de Koning J. P., M. R. Visser, G. A. Oelen, A. H. de Boer, ThW van der Mark, P. M. J. Coenegracht, ThFJ Tromp and H. W. Frijlink, (2001) Effect of Peak Inspiratory Flow and Flow Increase Rate on *In Vitro* Drug Deposition from Four Dry Powder Inhaler Devices, in *Dry Powder Inhalation: Technical and Physiological Aspects, Prescribing and Use,* Thesis, Rijksuniversiteit Groningen, Ch. 6., 83-94.

Finlay W., (2001) *The Mechanics of Inhaled Pharmaceutical Aerosols. An Introduction*, Academic Press, London.

French D. L., D. A. Edwards and R. W. Niven, (1996) The Influence of Formulation on Emission Deaggregation and Deposition of Dry Powders for Inhalation, *J. Aerosol Sci.*, 27(5), 769-783.

Hoe S., D. Traini, H-K. Chan, P. M. Young, (2009) Measuring charge and mass distributions in dry powder inhalers using the electrical Next Generation Impactor (eNGI), *European J. of Pharmaceutical Science*, 38, 88-94.

Islam N. and E. Gladki, (2008) Dry powder inhalers (DPIs) - A review of device reliability and innovation, Int. J. of Pharmaceutics, 360, 1-11.

Ligotke M. W., (2002) Development and characterization of a dry powder inhaler. In: *Dalby RN, Byron PR, Peart J, Farr SJ, editors. Respiratory drug delivery VIII, vol. I.* Tucson, AZ: Serentec Press Inc., 419–422.

Newman S. P. and W.W. Busse, (2002) Evolution of dry powder inhaler design, formulation, and performance, *Respir Med.,* 96(5), 293-304.

Olsson et al.: Patent Application Publication. Pub. No. US 2007/0107721 A1. Pub. Date: May, 17, 2007.

Schuler C., A. Bakshi, D. Tuttle, A. Smith, S. Paboojian, H. Snyder, D. Rasmussen, A. Clark, (1999) Inhale's dry-powder pulmonary drug delivery system: Challenges to current modeling of gas-solid flows. In: *Proceedings of FEDSM99: 3rd ASME/JSME joint fluids engineering conference* and *1999 ASME Fluids Engineering summer meeting*, FEDSM99-7895.

Tobyn M., J. N. Staniforth, D. Morton, Q. Harmer and M. E. Newton, (2004) Active and intelligent inhaler device development, *Int. J. of Pharmaceutics* 277, 31–37.

Tong Z. B., R. Y. Yang, K. W. Chu, A. B. Yu, S. Adi, H-K. Chan, (2010) Numerical study of the effects of particle size and polydispersity on the agglomerate dispersion in a cyclonic flow, *Chemical Engineering Journal* 164, 432–441.

Tsima M. P., G. P. Martin, C. Marriott, D. Gardenton and M. Yianneskis, (1994) Drug delivery to the respiratory tract using dry powder inhaler, *Int. J. of Pharmaceutics*, 101, 1-13.

Wetterlin K., (1988) Turbuhaler: A New Powder Inhaler for Administration of Drugs to the Airways. *Pharmaceutical Research*, 5(8), 506-508.

Zeng X-M, G. P. Martin, C. Marriott and J. Pritchard, (2000) The influence of carrier morphology on drug delivery by dry powder inhalers, *Int. J. of Pharmaceutics*, 200, 93–106.